Detectable anthropogenic influence in mean precipitation of China

Tao Wang, Ying Sun, Xuebin Zhang, Xiu-Qun Yang & Heyang Song

2025

Original citation:

Wang, T., Sun, Y., Zhang, X., Yang, X.-Q., & Song, H. (2025). Detectable anthropogenic influence in mean precipitation of China. *Geophysical Research Letters,* 52, e2025GL114870. https://doi.org/10.1029/2025GL114870

AGU ADVANCING EARTH AND SPACE SCIENCES

Geophysical Research Letters

RESEARCH LETTER
10.1029/2025GL114870

Detectable Anthropogenic Influence in Mean Precipitation of China

Tao Wang[1], Ying Sun[2], Xuebin Zhang[3], Xiu-Qun Yang[1], and Heyang Song[4]

[1]China Meteorological Administration Key Laboratory for Climate Prediction Studies, School of Atmospheric Sciences, Nanjing University, Nanjing, China, [2]State Key Laboratory of Climate System Prediction and Risk Management, China Meteorological Administration Key Laboratory for Climate Prediction Studies, National Climate Center, Beijing, China, [3]Pacific Climate Impacts Consortium, University of Victoria, Victoria, BC, Canada, [4]Chinese Academy of Meteorological Sciences, Beijing, China

Abstract Detecting and attributing regional-scale mean precipitation changes remains a challenging scientific problem. Due to significant spatiotemporal variability of precipitation changes and the limited ability of climate models to simulate these variations, attribution studies of China's mean precipitation changes remain scarce. We analyze China's long-term precipitation changes using four observational data sets and CMIP6 simulations, with percentage precipitation anomaly as a key metric. Through optimal fingerprinting detection, we identify anthropogenic signals in China's mean precipitation changes. Results reveal an increasing trend in annual precipitation across most regions since the 1960s, which CMIP6 models generally capture, though large inter-model discrepancies persist in simulating trends in southern China. Human influence on China's mean precipitation changes is detectable and separable from natural forcings. Anthropogenic signals are detected in three sub-climatic regions: Northwest China, Northeast China, and Tibetan Plateau. Three-signal analysis indicates that the increase in China's precipitation is primarily driven by greenhouse gas forcing.

Plain Language Summary Determining whether changes in mean precipitation are linked to human activities is difficult because they are largely influenced by natural climate variability, and current climate models cannot accurately simulate them. In this study, we analyze changes in mean precipitation in China using four observational data sets and the latest climate model simulations, with percentage precipitation anomaly as a metric. By applying an optimal fingerprinting method, we identify clear evidence of human influence on these changes. Results reveal that annual mean precipitation has been increasing across most parts of China since the 1960s. While climate models generally replicate this rising trend, they still show differences in simulating precipitation changes over southern China. Importantly, we find that human activities have distinctly influenced these changes, separate from natural climate factors. Further analysis indicates that the increase in mean precipitation is primarily driven by greenhouse gas emissions, which are partially offset by anthropogenic aerosols. Our study addresses the gap in the long-term attribution of mean precipitation in China, providing new evidence of significant human influence on one of the most important variables in the water cycle.

Key Points:

- Annual mean precipitation across most of China increased clearly from 1961 to 2020, a pattern that is generally captured by model simulations
- Using percentage precipitation anomaly, anthropogenic signal is detectable in China's mean precipitation, particularly in northern regions
- Greenhouse gas forcing drives increased mean precipitation and its effects are partially offset by influence of anthropogenic aerosols

Supporting Information:

Supporting Information may be found in the online version of this article.

Correspondence to:

Y. Sun and X.-Q. Yang,
sunying@cma.gov.cn;
xqyang@nju.edu.cn

Citation:

Wang, T., Sun, Y., Zhang, X., Yang, X.-Q., & Song, H. (2025). Detectable anthropogenic influence in mean precipitation of China. *Geophysical Research Letters*, *52*, e2025GL114870. https://doi.org/10.1029/2025GL114870

Received 18 JAN 2025
Accepted 7 JUN 2025

Author Contributions:

Conceptualization: Ying Sun
Data curation: Tao Wang, Ying Sun, Xuebin Zhang
Formal analysis: Tao Wang
Funding acquisition: Ying Sun
Investigation: Tao Wang
Methodology: Xuebin Zhang, Heyang Song
Supervision: Xiu-Qun Yang
Visualization: Tao Wang
Writing – original draft: Tao Wang
Writing – review & editing: Ying Sun, Xiu-Qun Yang

1. Introduction

Detection and attribution of mean precipitation are crucial for understanding the major drivers of water cycle under global warming. However, because of high dependence of mean precipitation on natural variability at various temporal and spatial scales, detecting human influence on regional precipitation has been a very challenging topic. Research has shown that anthropogenic forcing has significantly affected the pattern of global land precipitation since the 20th century and human activities have notably driven increased precipitation in the mid- to high-latitude regions of the Northern Hemisphere (Alkama, 2014; Noake et al., 2012; X. Zhang et al., 2007). Subsequent studies suggest that while greenhouse gases are likely the primary driver of past changes in global total precipitation, the spatial distribution of precipitation changes has been strongly influenced by anthropogenic aerosol emissions (Min et al., 2008; C. Wang, 2015). The IPCC Sixth Assessment Report (AR6) concludes that "globally averaged land precipitation has likely increased since the middle of the 20th century," and it is likely that human influence has contributed to large-scale precipitation changes observed since the mid-20th century (IPCC, 2021). Though subsequent detection and attribution studies have investigated many precipitation-related metrics such as the extreme precipitation, very few studies have focused on mean precipitation.

Since the 1960s, China's mean precipitation has exhibited an overall increasing trend (CMA, 2021), characterized by significant interannual and interdecadal variability. Regionally, precipitation increases are most evident along the southeastern coast, the Tibetan Plateau, and Northwest China, whereas decreases are observed in Southwest and North China (B. Li et al., 2016; Liang et al., 2011; A. Zhang & Zhao, 2022). Existing studies primarily explore the possible mechanisms of these changes from the perspective of internal variability, pointing out that the sea surface temperature, land surface processes and snow cover over the Tibetan Plateau are all important factors influencing precipitation changes (Ding et al., 2008; Z. Zhang et al., 2018; Zhao et al., 2022). These factors affect atmospheric circulation, including the Asian monsoon, the subtropical high pressure in the northwestern Pacific, and large-scale moisture transport through thermal and dynamic processes, thereby driving the interannual and interdecadal variation in precipitation (L. Sun et al., 2021; G. Wu et al., 2015; Y. Zhang et al., 2022).

Research on the external forcings driving changes in China's mean precipitation remains scarce. Limited studies have mainly focused on the detection and attribution of extreme precipitation, revealing that human activities have contributed to changes in the frequency and intensity of extreme precipitation in China (W. Chen et al., 2024; Dong et al., 2022). W. Li and Chen (2021) have identified an increasing trend of China's annual total precipitation (PRCPTOT) during 1961–2017 through a field significance test. J. Zhang et al. (2019) quantified the impacts of human activities and natural external forcings on China's atmospheric precipitable water and robustly detected the influence of anthropogenic forcing (ANT). However, changes in atmospheric humidity do not directly correspond to changes in precipitation (Allen & Ingram, 2002; Held & Soden, 2006).

The major challenges in detecting and attributing mean precipitation changes stem from the significant influence of natural internal variability and the limited capability of current climate models to accurately simulate precipitation. Sarojini et al. (2016) have suggested that developing and using new metrics in detection and attribution studies could be more effective in identifying key features of precipitation changes, rather than solely relying on model improvements or waiting for climate change signals to further strengthen. Existing studies have shown that using climatological percentage indices help reduce discrepancies between model simulations and observed trends, while also effectively enhancing the signal-to-noise ratio (Noake et al., 2012; Z. Wang et al., 2023).

To fill in the gap in the attribution of long-term changes in mean precipitation in China, we investigate the mean precipitation change based on percentage precipitation anomaly (PPA), and the model responses to different external forcings using multiple observational data sets and CMIP6 simulations. The optimal fingerprint method is applied to detect and attribute the impacts of various external forcing factors in China and its seven sub-climate regions. The rest of this paper is organized as follows. Section 2 introduces the data sets and research methods, Section 3 provides the results of the detection and attribution analysis, and Section 4 summarizes and discusses the key findings of the study.

2. Data and Methods

This study uses four observational precipitation data sets: (a) The homogenized daily precipitation observational data set from 2,419 surface meteorological stations in China, provided by the National Meteorological Information Center of the China Meteorological Administration (CMA) (Cao et al., 2016); (b) The CN05 data set, interpolated from 2,419 stations with a horizontal resolution of 0.25° × 0.25° (J. Wu & Gao, 2013); (c) The Global Precipitation Climatology Centre (GPCC v2.1) global monthly mean precipitation data set, with a resolution of 2.5° × 2.5° (Schneider et al., 2014); and (d) The global monthly precipitation reconstruction data set over land (PREC/L), provided by the National Oceanic and Atmospheric Administration (NOAA), with a resolution of 2.5° × 2.5°(M. Chen et al., 2002).

To ensure data continuity and integrity, CMA station data are pre-processed through selection and gridding. Stations with record coverage exceeding 75% between 1961 and 2020 are selected, yielding a total of 2,261 stations. The PPA relative to the 1961–1990 climatology is calculated for each station, followed by gridding and regional averaging. This method effectively emphasizes regional precipitation patterns and enhances the identification of anomalous precipitation events (Z. Wang et al., 2023). For other observational data sets, PPA are directly calculated at the interpolated grid points. To facilitate comparisons across different observational data sets and reduce the impact of resolution differences, all other observational data are interpolated to a uniform resolution of 2° × 2°. A masking process, based on the gridded CMA station data, is applied to ensure uniformity in the number of grid points across all data sets. Sensitivity tests confirm that different masking approaches or

processing methods for station data have no impact on the qualitative conclusions of the subsequent detection and attribution analysis.

Model data are derived from the DAMIP simulations of CMIP6 (Gillett et al., 2016). Climate models that included at least three members under the combined anthropogenic and natural forcings (ALL), greenhouse gas forcing (GHG), anthropogenic aerosol forcing (AER), and natural forcing (NAT) experiments are selected for subsequent detection and attribution analysis (Table S1 in Supporting Information S1). The study period spans 1961–2020. Since ALL simulation data from CMIP6 extend only to 2014, data from the SSP2-4.5 scenario are used to extend the series to 2020. Results from the preindustrial control (CTL) simulations in CMIP6 are used to estimate the internal variability of the climate system. Similarly, model precipitation data are interpolated to a uniform resolution of $2° \times 2°$ and masked based on the gridded CMA station data set. The calculation of PPA in the models follows the same methodology as that applied to gridded observational data.

This study applies the optimal fingerprint method based on Total Least Squares (Allen & Stott, 2003; Ribes et al., 2013) to conduct detection and attribution analysis of the long-term trends in regional precipitation across China. This method essentially involves regressing observed changes onto the responses to specific forcings estimated from model data, expressed as: $Y = (X - v) \times \beta + \varepsilon$, where Y represents the observed changes in the climate variable, X denotes the signal patterns, v accounts for internal variability within the signal patterns, β is the scaling factor, and ε represents the residual vector representing the component of observed internal variability that cannot be explained by the signal.

In the detection and attribution analyses, we reduce the spatial and temporal dimensions of both observational and model data so that the noise covariance matrix is full rank. The time series of regional averages for 1961–2020 is processed using a 5-year non-overlapping average, resulting in 12 time points for analysis. The Multi-Model Ensemble (MME) is constructed by first averaging multiple simulations (runs) for each model, followed by an ensemble averaging of all model results. CTL simulations are divided into even 60-year segments, matching the observation period. One segment is used for optimal estimation of the scaling factor β, while another is used to calculate the 5%–95% confidence interval for β and to perform a residual consistency test to validate the model assumptions (Ribes et al., 2013). When the 90% uncertainty range of the scaling factor is above zero, the corresponding signal is considered detected. In contrast, if the 90% confidence interval of the scaling factor include zero, it means the signal could not be detected.

We conduct single-, two-, and three-signal analyses to explore the influences and contributions of various external forcings on regional precipitation changes in China. In the one-signal analysis, observed precipitation changes are regressed onto the ALL forcing signal to access the combined effects of all external forcings. The two-signal analysis simultaneously regresses the observations onto the ANT and NAT signals to separate the relative contributions of human activities and natural variability. The three-signal analysis examines the GHG, AER, and NAT signals by regressing observations onto these three signals simultaneously to determine whether they can be effectively detected and separated.

3. Results

3.1. Mean Precipitation Changes From Observations and Model Simulations

Figure 1 displays the spatial patterns of linear trends in PPA across China from 1961 to 2020, based on four observational data sets, along with the regionally averaged time series. Four data sets exhibit generally consistent spatial patterns of PPA trends, with most regions in China experiencing an increase in precipitation, while a zonal band stretching from Southwest to North China shows a decreasing trend. The most significant increase in precipitation is observed in Northwest China, with notable growth rates also present in Northeast China and the southeastern coastal regions. The regionally averaged time series (Figure 1e) reveals an overall upward trend in PPA over the past decades across all four data sets, with a sharper increase since the early 21st century, aligning with earlier findings (CMA, 2021). However, the magnitude of change varies among data sets. The station and GPCC data sets show higher rates of increase, at 4.22%/decade and 4.15%/decade, respectively, while CN05 and NOAA exhibit lower trends, at 2.77%/decade and 2.65%/decade, respectively. Our gridding method for station data better captures regional precipitation characteristics, particularly extreme precipitation, leading to a higher growth rate in the station data. The elevated growth rate in the GPCC data set is largely due to anomalously high precipitation values in 2020 (Figure S1 in Supporting Information S1).

10.1029/2025GL114870

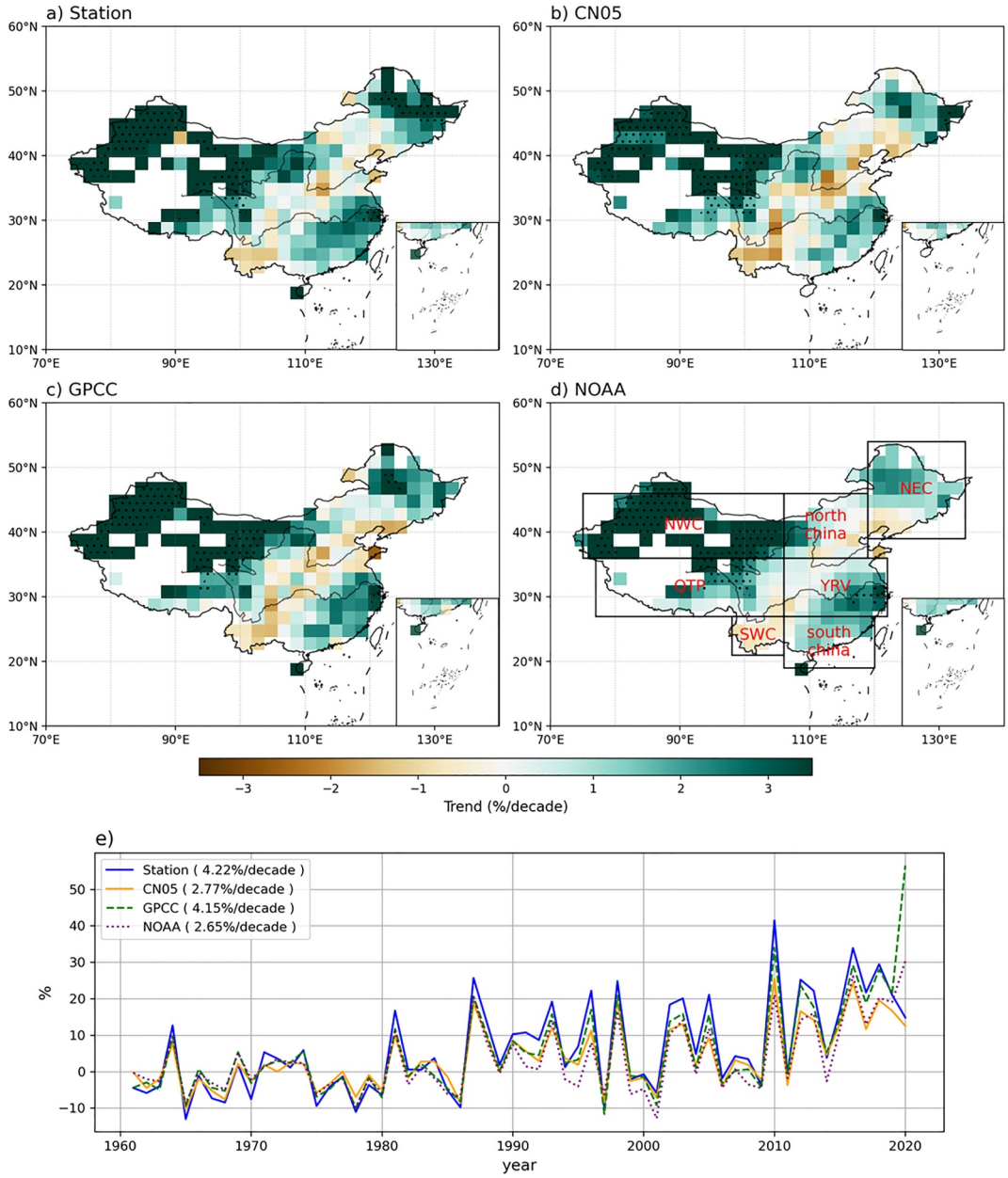

Figure 1. Spatial distribution of the linear trends in percentage precipitation anomaly (PPA) (units: %/decade) across China from 1961 to 2020, based on four observational data sets: (a) station data, (b) CN05, (c) GPCC, and (d) NOAA. Panel (d) also illustrates the division of China into seven sub-climate regions. PPA (relative to the 1961–1990 average) averaged over China under four observations are shown on the bottom panel (e).

Figures 2a–2d shows the spatial distribution of PPA trends across China under the ALL, GHG, AER, and NAT forcing, based on the MME. The results indicate that the simulated precipitation responses are generally weaker than the observed changes. Under ALL forcing, the models capture a general increasing trend in precipitation over northern China, which is broadly consistent with observations. However, in southeastern China, the simulated trends deviate from the observations, showing an opposite direction. The GHG simulations demonstrate that greenhouse gas emissions drive the increasing precipitation trends over China, whereas the AER simulations highlight the suppressive effect of anthropogenic aerosol emissions on precipitation, particularly in southern China. The response to NAT forcing is weak overall, indicating its little contribution to the observed changes.

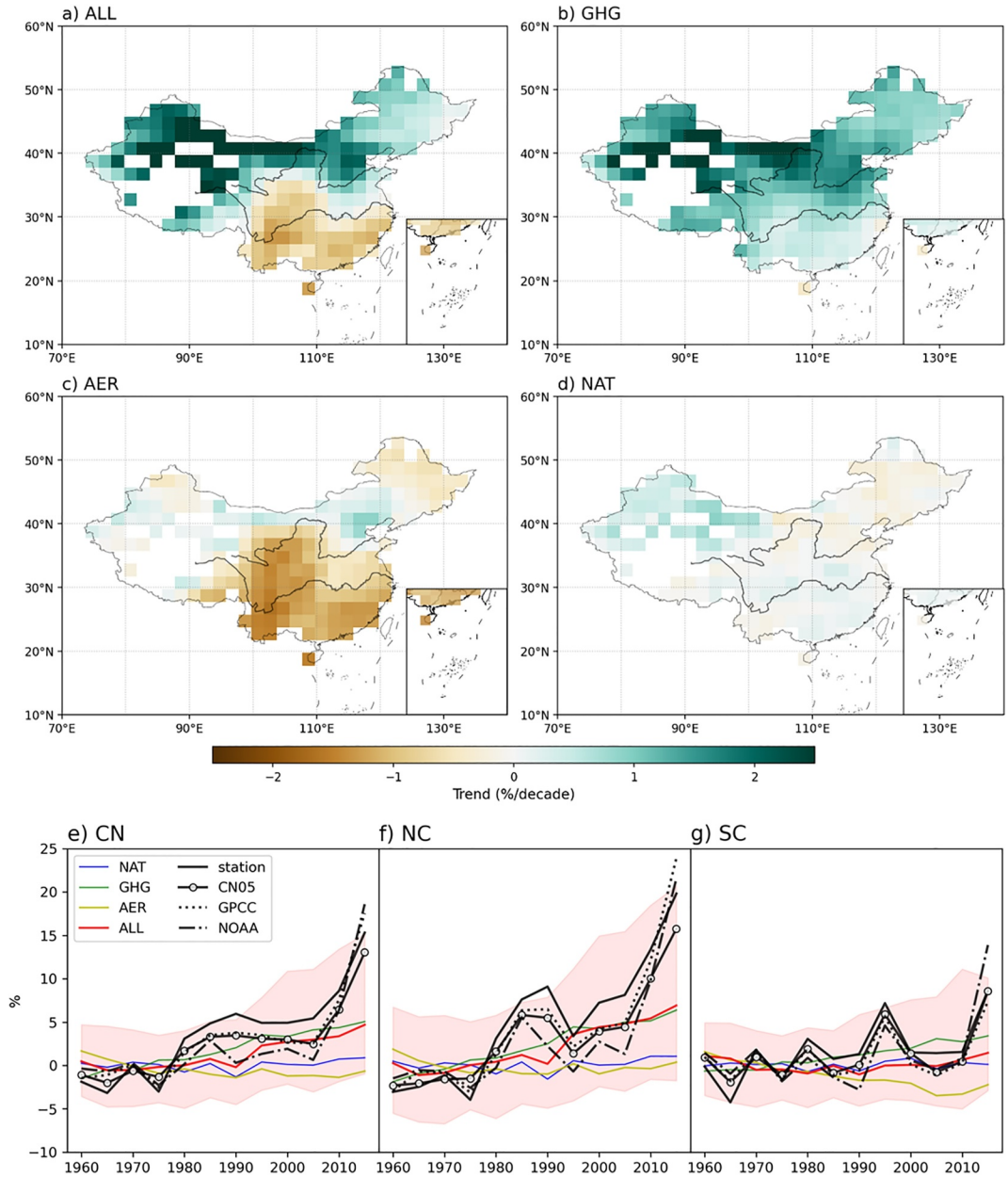

Figure 2. Spatial distribution of trends in percentage precipitation anomaly (PPA) (relative to the 1961–1990 average) for the 1961–2020 period (units: %/decade) from the CMIP6 multi-model response to the (a) ALL, (b) GHG, (c) AER, and (d) NAT forcings. Time series of PPA averaged over (e) China, (f) northern China, and (g) southern China from various observational data sets (black lines) and CMIP6 multi-model responses to ALL (red), GHG (green), AER (orange), and NAT (blue) forcings. The light pink shading represents the 5%–95% range of individual model results under ALL forcings.

The discrepancies in mean precipitation changes between the ALL forcing and observations in southeastern China highlight significant inter-model differences, limited model accuracy in simulating mean precipitation, and a low signal-to-noise ratio. In the analyzed models, the majority of members in the historical experiments exhibit negative trends in SC region, with only about one-third showing an increasing trend in the SC region (Figure S2a in Supporting Information S1). For both ensemble results from all the models (Figure 2g) and from the model members with the positive precipitation trend in SC (Figure S2b in Supporting Information S1), the variability in mean precipitation is considerably larger than the linear trend, indicating a very weak signal relative to the background noise in SC. These discrepancies may also be related to the models' ability to accurately reproduce

different categories of precipitation. In eastern China, the sharp rise in anthropogenic aerosols over recent decades has suppressed light precipitation (Liu et al., 2019). While the AER simulations successfully reproduce this effect, the models fail to capture the increase in heavy precipitation in southeastern China. Additionally, multi-timescale variability driven by natural internal processes may dominate regional precipitation changes, further complicating the comparison of trends between models and observations (Dai & Bloecker, 2019).

Figures 2e–2g shows the 5-year non-overlapping mean time series of PPA from observational data and model simulations for three regions: CN (nationwide), NC (northern China, north of 35°N), and SC (southern China, south of 35°N). Despite numerical differences among the data sets, they exhibit strong consistency in overall trends and interdecadal variations. Notably, the station data show higher PPA values compared to other data sets, primarily because the gridding process smooths extreme precipitation values from stations, and the 5-year non-overlapping mean further reduces interannual variability. All observational data sets reveal significant increasing PPA trends for the CN and NC regions, while the SC region shows a relatively weaker increasing trend. In the model simulations, the MME results capture the overall increasing trend observed in precipitation but fail to reproduce the interdecadal variability. Under ALL forcing, the range of model-simulated precipitation changes encompasses the observed precipitation changes for all regions. Both CN and NC show increasing PPA trends, while SC exhibits minimal changes. GHG forcing results in increasing PPA across all regions, while AER forcing causes decreases in PPA. NAT forcing, on the other hand, does not produce significant changes in precipitation trends.

3.2. Detection and Attribution of Mean Precipitation Changes in China

Figure 3 shows the detection and attribution results for PPA in the CN, NC, and SC regions based on four observational data sets. In the single- and two-signal analyses (Figure 3a), the confidence intervals of the scaling factors for the ALL and ANT signals in the CN and NC regions are significantly greater than 0, indicating that the influence of anthropogenic external forcings can be detected in these regions. However, the wide range of the scaling factors reflects some uncertainty in the detection results. In the SC region, none of the four data sets detects a significant anthropogenic external forcing signal because the confidence intervals of scaling factors include zero. This means the precipitation long-term trend in the SC region is still weak compared with the noise. The NAT signal is undetectable in most cases or exhibits large uncertainty ranges. Across the one and two-signal analyses, the four observational data sets show a high degree of consistency in detection results, differing only in the magnitude of the scaling factors. This consistency demonstrates the robustness and reliability of the detection results. Regarding the differences between the station and CN05 data sets, when station data are used to mask CN05, many grid points in Northwest and Tibetan Plateau, where significant precipitation increases occur, are excluded. This leads to smaller overall PPA values for CN05 in the NC region and, consequently, smaller scaling factors for the ALL and ANT signals compared to those in the station data. Similar conclusions have been reported in previous studies using these two data sets to analyze extreme precipitation in China (Dong et al., 2022).

Figure 3b shows the three-signal results for the GHG, AER, and NAT signals. In the CN region, the GHG signal is consistently detectable across all four data sets. The AER signal is also detectable in all data sets except CN05, though the scaling factors exhibit considerable uncertainty. In the NC region, the GHG signal is detected in all four data sets, while the AER signal is only detected in the GPCC data set. In the SC region, both the GHG and AER signals are detected. The NAT signal, however, remains undetectable in any of the cases. Compared to the one- and two-signal analyses, the three-signal detection results exhibit greater differences and uncertainties across four observational data sets, indicating that three-signal detection remains uncertain at the regional scale.

Figures 3c and 3d further illustrates the contributions of different external forcings to PPA trends in the CN and NC regions, calculated by multiplying the linear PPA trends for each forcing (ALL, GHG, AER, and NAT) by their corresponding scaling factors, derived from single-signal (ALL) and three-signal (GHG, AER, and NAT) analyses, based on four observational data sets. During 1961–2020, the observed increases in PPA for CN across the four data sets (station, CN05, GPCC, NOAA) range from 17.1% to 29.7% (90% confidence interval), 7.0%–16.3%, 8.9%–24.6%, and 5.5%–17.3%, respectively. Of these increases, the portion attributable to ALL forcing ranges from 18.3%–23.8%, 10.4%–14.7%, 20.2%–25.9%, and 13.4%–19.0%, respectively. The GHG forcing contributes to increases in PPA of 14.0%–42.8%, 6.0%–25.1%, 32.9%–108.0%, and 16.6%–63.1%, respectively, across the four data sets. The AER signal is detected only in the GPCC and NOAA data sets, where its effect

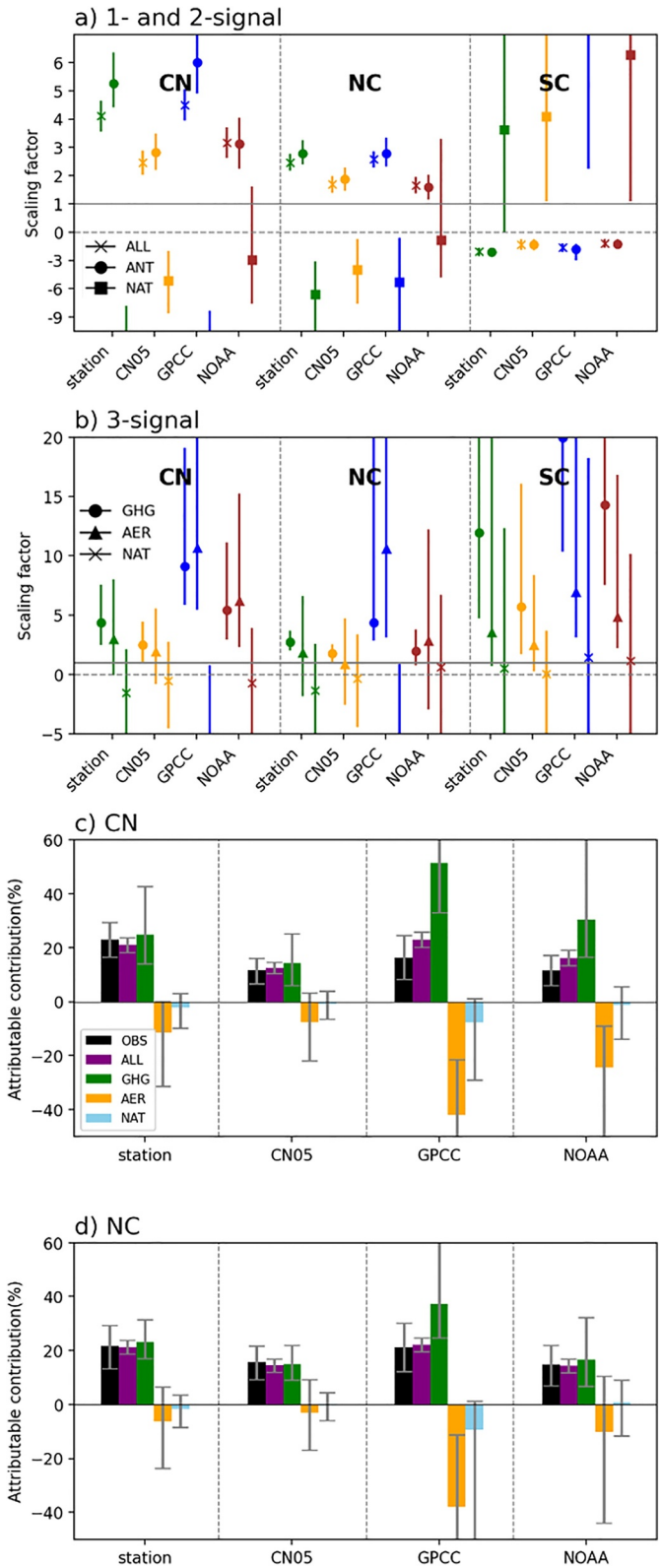

Figure 3.

offsets the precipitation increases driven by GHG forcing. None of the data sets detect any contribution from NAT forcing. The results for the NC region closely resemble those for the CN region, exhibiting similar trends and contributions from external forcings. These findings quantitatively highlight the dominant role of GHG forcing in driving precipitation increases across China, particularly in northern regions.

3.3. Detection and Attribution in the Seven Sub-Climate Regions of China

Figures 4a–4g presents the 5-year non-overlapping mean time series of PPA for observational data and model simulations across China's seven sub-climate regions (as shown in Figure 1d). Only the results based on station observational data are shown here, as the qualitative results from other data sets are largely similar. The observational results indicate increasing PPA trends in the NWC, NEC, QTP, YRV, and South China regions, a decreasing trend for SWC, and no significant trend for North China. In most regions, the trends under ALL forcing are relatively consistent with the observational results. However, in the YRV and South China regions, the simulated trends under ALL forcing contradict the observed trends, suggesting that other factors including internal variability play significant role in these two regions and may dominate precipitation changes on interdecadal scales. Furthermore, GHG forcing consistently leads to increased regional precipitation across almost all regions, whereas AER forcing suppresses these increases. NAT forcing shows negligible trends.

Figure 4h shows the detection and attribution results from one- and two-signal analyses for China's seven sub-climate regions over 1961–2020. The ALL and ANT signals are robustly detected in the NWC, NEC, and QTP regions, with the confidence intervals of scaling factors significantly above 0, indicating a clear influence of human activities on precipitation changes in these areas. In contrast, in southern regions such as YRV, SWC, and South China, neither the ALL nor ANT signals are detected. This outcome reflects biases in model simulations as well as the strong influence of internal variability, which obscures the detectable responses to external forcings. Furthermore, the NAT signal is not detected in most regions except for South China. Results from the three-signal analysis reveal that the GHG signal is detectable in the NWC, NEC, QTP, and YRV regions, while the AER signal is only detected in the QTP region. These findings suggest that greenhouse gas emissions are the primary driver of precipitation changes in northern and plateau regions of China, whereas in southern regions, their influence is not effectively detected compared to the impact of internal variability.

Figure 3. Panel (a, b) shows the best estimates of scaling factors and their 5%–95% confidence intervals for China (left), northern China (center), and southern China (right) from single-, two-, and three-signal analyses, based on different observational data sets for the 1961–2020 period. In each panel, different colors represent various observational data sets, and the markers at the center of the error bars indicate the different forcings. Panels (c, d): Display the attributable contributions of ALL, GHG, AER, and NAT forcings to the observed trend (OBS) in percentage precipitation anomaly for CN and NC over the 1961–2020 period, along with their 5%–95% confidence intervals (error bars). These contributions are derived from single-signal and three-signal analyses. The confidence intervals for the linear trends in observed precipitation changes are estimated using the bootstrap method.

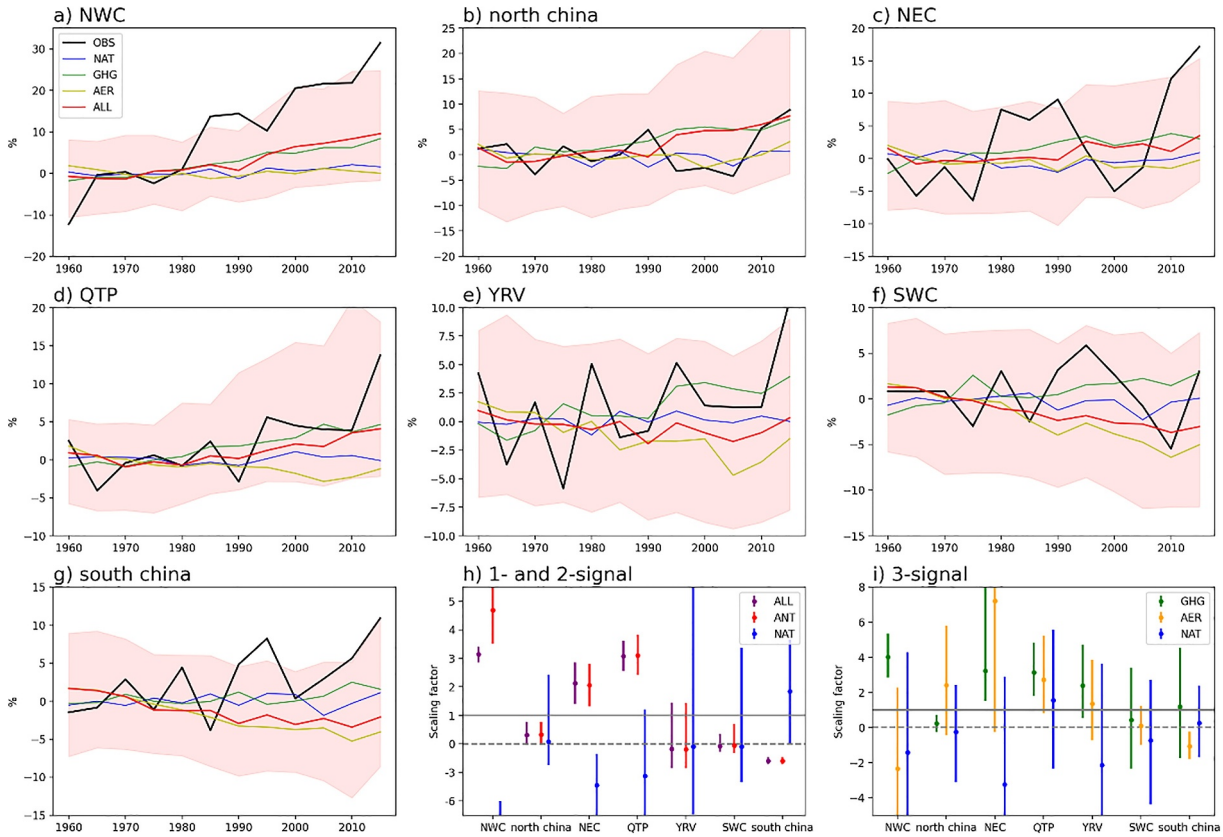

Figure 4. Panels (a–g): Time series of percentage precipitation anomaly averaged over seven sub-climate regions, using the China Meteorological Administration (CMA) station data set (black lines) and CMIP6 multi-model responses to ALL (red), GHG (green), AER (orange), and NAT (blue) forcings. The light pink shading represents the 5%–95% range of individual model results under ALL forcings. Panel (h): Displays results from single-signal analyses for the ALL (purple) forcing and two-signal analyses for ANT (red) and NAT (blue) forcings. Panel (i): Shows results from three-signal analyses involving GHG (green), AER (yellow), and NAT (blue) forcings, based on the CMA station data set.

4. Conclusion and Discussion

The influence of human activities on mean precipitation changes remains underexplored in climate change detection and attribution research (IPCC, 2021; Y. Sun et al., 2022). This study analyzes annual mean precipitation changes in China from 1961 to 2020 using the PPA metric, which partially corrects model biases in climatic backgrounds across regions (e.g., varying levels of aridity and humidity), thereby more effectively capturing common trends in precipitation changes. During regional averaging, PPA preserves the relative magnitude of precipitation changes, allowing for a more balanced representation of changes across regions with diverse precipitation intensities and thereby effectively enhancing the detectability of regional signals (Figure S3 in Supporting Information S1).

Results indicate that China's mean precipitation has increased since the 1960s. While the MME simulations tend to underestimate these trends, models generally reproduce the positive trends of observed precipitation. In further analysis, we conduct detection and attribution analysis of China's mean precipitation based on four different observational data sets. All data sets consistently show that the ALL and ANT signals can be detected across China. The three-signal analysis further reveals that the increase in China's mean precipitation is predominantly driven by greenhouse gas emissions, whereas the impact of anthropogenic aerosols is not detectable when compared to internal variability. At the sub-climate scale, ANT signals are reliably detected in the NWC, NEC, and QTP regions.

Southern China lies within the East Asian monsoon region, where precipitation exhibits significant variability across multi-timescale due to the complex interactions among various components of the climate system (J. Chen et al., 2014; Gu et al., 2018). However, current models perform poorly in simulating precipitation trends in this

region, and substantial inter-model discrepancies further complicate the detection of external forcing signals. As emissions increase in the future, precipitation in southern China is projected to exhibit a clear upward trend (Figure S4 in Supporting Information S1), indicating that although the anthropogenic signal was weak during the historical period, it is expected to strengthen with increasing emissions.

Overall, this study robustly detects anthropogenic signals in China's mean precipitation for the first time and highlights the critical role of greenhouse gas emissions in driving precipitation changes. We also analyze mean precipitation changes in China's sub-climate regions, providing valuable insights to inform more targeted and regionally specific climate adaptation policies. Our findings offer new evidence of the significant role of human activities in changes in mean precipitation across China.

Data Availability Statement

The station data and CN05 data analyzed during the current study are not publicly available for legal/ethical reasons but are available from the corresponding author on reasonable request. GPCC global monthly mean precipitation data set are available at https://climatedataguide.ucar.edu/climate-data/gpcc-global-precipitation-climatology-centre. NOAA's Precipitation Reconstruction over Land (PREC/L) are available at http://www.psl.noaa.gov/data/gridded/data.precl.html. The CMIP6 model simulation data are available at https://esgf-node.llnl.gov/search/cmip6/.

Acknowledgments
This study was supported by the National Natural Science Foundation of China (42025503 and U2342228) and the Key Innovation Team of China Meteorological Administration "Climate Change Detection and Response" (CMA2022ZD03).

References

Alkama, R. (2014). Human influence on changes in the distribution of land precipitation. *Journal of Hydrology*, *511*, 589–593. https://doi.org/10.1016/j.jhydrol.2014.02.016

Allen, M. R., & Ingram, W. J. (2002). Constraints on future changes in climate and the hydrologic cycle. *Nature*, *419*(6903), 224–232. https://doi.org/10.1038/nature01092

Allen, M. R., & Stott, P. A. (2003). Estimating signal amplitudes in optimal fingerprinting, part I: Theory. *Climate Dynamics*, *21*(5–6), 477–491. https://doi.org/10.1007/s00382-003-0313-9

Cao, L., Zhu, Y., Tang, G., Yuan, F., & Yan, Z. (2016). Climatic warming in China according to a homogenized data set from 2419 stations: Climatic warming in China. *International Journal of Climatology*, *36*(13), 4384–4392. https://doi.org/10.1002/joc.4639

Chen, J., Wen, Z., Wu, R., Chen, Z., & Zhao, P. (2014). Interdecadal changes in the relationship between Southern China winter-spring precipitation and ENSO. *Climate Dynamics*, *43*(5–6), 1327–1338. https://doi.org/10.1007/s00382-013-1947-x

Chen, M., Xie, P., Janowiak, J. E., & Arkin, P. A. (2002). Global land precipitation: A 50-yr monthly analysis based on gauge observations. *Journal of Hydrometeorology*, *3*(3), 249–266. https://doi.org/10.1175/1525-7541(2002)003<0249:GLPAYM>2.0.CO;2

Chen, W., Cui, H., Zwiers, F. W., Li, C., & Zheng, J. (2024). Detection and attribution of changes in precipitation extremes in China and its different climate zones. *Journal of Climate*, *37*(20), 5373–5385. https://doi.org/10.1175/JCLI-D-23-0770.1

CMA. (2021). *Blue book on climate change in China (2021)*. Science Press.

Dai, A., & Bloecker, C. E. (2019). Impacts of internal variability on temperature and precipitation trends in large ensemble simulations by two climate models. *Climate Dynamics*, *52*(1–2), 289–306. https://doi.org/10.1007/s00382-018-4132-4

Ding, Y., Wang, Z., & Sun, Y. (2008). Inter-decadal variation of the summer precipitation in East China and its association with decreasing Asian summer monsoon. Part I: Observed evidences. *International Journal of Climatology*, *28*(9), 1139–1161. https://doi.org/10.1002/joc.1615

Dong, S., Sun, Y., & Zhang, X. (2022). Attributing observed increase in extreme precipitation in China to human influence. *Environmental Research Letters*, *17*(9), 095005. https://doi.org/10.1088/1748-9326/ac888e

Gillett, N. P., Shiogama, H., Funke, B., Hegerl, G., Knutti, R., Matthes, K., et al. (2016). The detection and attribution model intercomparison project (DAMIP v1.0) contribution to CMIP6. *Geoscientific Model Development*, *9*(10), 3685–3697. https://doi.org/10.5194/gmd-9-3685-2016

Gu, W., Wang, L., Hu, Z.-Z., Hu, K., & Li, Y. (2018). Interannual variations of the first rainy season precipitation over South China. *Journal of Climate*, *31*(2), 623–640. https://doi.org/10.1175/JCLI-D-17-0284.1

Held, I. M., & Soden, B. J. (2006). Robust responses of the hydrological cycle to global warming. *Journal of Climate*, *19*(21), 5686–5699. https://doi.org/10.1175/JCLI3990.1

IPCC. (2021). *Climate change 2021 – The physical science basis: Working group I contribution to the sixth assessment report of the intergovernmental panel on climate change* (1a ed.). Cambridge University Press. https://doi.org/10.1017/9781009157896

Li, B., Chen, Y., Chen, Z., Xiong, H., & Lian, L. (2016). Why does precipitation in northwest China show a significant increasing trend from 1960 to 2010? *Atmospheric Research*, *167*, 275–284. https://doi.org/10.1016/j.atmosres.2015.08.017

Li, W., & Chen, Y. (2021). Detectability of the trend in precipitation characteristics over China from 1961 to 2017. *International Journal of Climatology*, *41*(S1), E1980–E1991. https://doi.org/10.1002/joc.6826

Liang, L., Li, L., & Liu, Q. (2011). Precipitation variability in Northeast China from 1961 to 2008. *Journal of Hydrology*, *404*(1–2), 67–76. https://doi.org/10.1016/j.jhydrol.2011.04.020

Liu, S., Xing, J., Zhao, B., Wang, J., Wang, S., Zhang, X., & Ding, A. (2019). Understanding of aerosol–climate interactions in China: Aerosol impacts on solar radiation, temperature, cloud, and precipitation and its changes under future climate and emission scenarios. *Current Pollution Reports*, *5*(2), 36–51. https://doi.org/10.1007/s40726-019-00107-6

Min, S.-K., Zhang, X., & Zwiers, F. (2008). Human-induced Arctic moistening. *Science*, *320*(5875), 518–520. https://doi.org/10.1126/science.1153468

Noake, K., Polson, D., Hegerl, G., & Zhang, X. (2012). Changes in seasonal land precipitation during the latter twentieth-century. *Geophysical Research Letters*, *39*(3), 2011GL050405. https://doi.org/10.1029/2011GL050405

Ribes, A., Planton, S., & Terray, L. (2013). Application of regularised optimal fingerprinting to attribution. Part I: Method, properties and idealised analysis. *Climate Dynamics*, *41*(11–12), 2817–2836. https://doi.org/10.1007/s00382-013-1735-7

Sarojini, B. B., Stott, P. A., & Black, E. (2016). Detection and attribution of human influence on regional precipitation. *Nature Climate Change*, *6*(7), 669–675. https://doi.org/10.1038/nclimate2976

Schneider, U., Becker, A., Finger, P., Meyer-Christoffer, A., Ziese, M., & Rudolf, B. (2014). GPCC's new land surface precipitation climatology based on quality-controlled in situ data and its role in quantifying the global water cycle. *Theoretical and Applied Climatology*, *115*(1–2), 15–40. https://doi.org/10.1007/s00704-013-0860-x

Sun, L., Yang, X.-Q., Tao, L., Fang, J., & Sun, X. (2021). Changing impact of ENSO events on the following summer rainfall in eastern China since the 1950s. *Journal of Climate*, *34*(20), 8105–8123. https://doi.org/10.1175/JCLI-D-21-0018.1

Sun, Y., Zhang, X., Ding, Y., Chen, D., Qin, D., & Zhai, P. (2022). Understanding human influence on climate change in China. *National Science Review*, *9*(3), nwab113. https://doi.org/10.1093/nsr/nwab113

Wang, C. (2015). Anthropogenic aerosols and the distribution of past large-scale precipitation change. *Geophysical Research Letters*, *42*(24), 10876–10884. https://doi.org/10.1002/2015GL066416

Wang, Z., Sun, Y., Zhang, X., Li, T., Li, C., Min, S.-K., & Hu, T. (2023). Human influence on historical heaviest precipitation events in the Yangtze River Valley. *Environmental Research Letters*, *18*(2), 024044. https://doi.org/10.1088/1748-9326/acb563

Wu, G., Duan, A., Liu, Y., Mao, J., Ren, R., Bao, Q., et al. (2015). Tibetan Plateau climate dynamics: Recent research progress and outlook. *National Science Review*, *2*(1), 100–116. https://doi.org/10.1093/nsr/nwu045

Wu, J., & Gao, X. (2013). A gridded daily observation dataset over China region and comparison with the other datasets. *Chinese Journal of Geophysics*, *56*(4), 1102–1111. https://doi.org/10.6038/cjg20130406

Zhang, A., & Zhao, X. (2022). Changes of precipitation pattern in China: 1961–2010. *Theoretical and Applied Climatology*, *148*(3–4), 1005–1019. https://doi.org/10.1007/s00704-022-03986-w

Zhang, J., Zhao, T., Dai, A., & Zhang, W. (2019). Detection and attribution of atmospheric precipitable water changes since the 1970s over China. *Scientific Reports*, *9*(1), 17609. https://doi.org/10.1038/s41598-019-54185-z

Zhang, X., Zwiers, F. W., Hegerl, G. C., Lambert, F. H., Gillett, N. P., Solomon, S., et al. (2007). Detection of human influence on twentieth-century precipitation trends. *Nature*, *448*(7152), 461–465. https://doi.org/10.1038/nature06025

Zhang, Y., Zhou, W., Wang, X., Wang, X., Zhang, R., Li, Y., & Gan, J. (2022). IOD, ENSO, and seasonal precipitation variation over Eastern China. *Atmospheric Research*, *270*, 106042. https://doi.org/10.1016/j.atmosres.2022.106042

Zhang, Z., Sun, X., & Yang, X.-Q. (2018). Understanding the interdecadal variability of East Asian summer monsoon precipitation: Joint influence of three oceanic signals. *Journal of Climate*, *31*(14), 5485–5506. https://doi.org/10.1175/JCLI-D-17-0657.1

Zhao, Y., Cheng, J., Feng, G., Zhi, R., Zheng, Z., & Zhang, Z. (2022). Analysis of the atmospheric direct dynamic source for the westerly extended WPSH and record-breaking Plum Rain in 2020. *Climate Dynamics*, *59*(3–4), 1233–1251. https://doi.org/10.1007/s00382-022-06186-4